Strength and deflection behavior of spun concrete poles with CFRP reinforcement

Ashraf M. Shalaby,
Fouad H. Fouad,
and Ronald Albanese

Editor's quick points

- Carbon-fiber-reinforced polymer (CFRP) composites show potential as a replacement for steel reinforcement because of their corrosion resistance, high strength, and light weight.
- This research studied the strength and deflection behavior of spun concrete poles with CFRP reinforcement.
- The performance of the poles reinforced with CFRP bars was satisfactory under bending loads, which are the primary governing loads in most applications.

Carbon-fiber-reinforced polymer (CFRP) reinforcement shows immense potential in civil engineering applications as an alternative to traditional steel reinforcement because of its unique properties. CFRP is high strength, lightweight, noncorrosive, and nonmagnetic. The improved durability of CFRP-reinforced concrete has caused CFRP to gain considerable use and attention in the reinforced concrete field.

Most research on the use of CFRP in concrete structures has focused on the rectangular and tee cross-sectional shapes commonly used in buildings and bridges. Limited information, however, is available in the literature on circular concrete sections reinforced with CFRP.[1–4] Terrasi and Lees tested centrifugally cast high-strength concrete poles reinforced with CFRP wires manufactured in Switzerland. Their weight was about 30% less than for comparable conventional steel reinforced concrete poles.[2]

Members with circular cross sections are commonly used in the precast concrete industry for poles, piles, pipes, and columns for buildings and bridge piers. Round spun concrete poles are used in supporting electric transmission lines, communication towers, stadium lighting, and a variety of other applications. The round cross section, which is dictated by the manufacturing process in the case of spun concrete, offers a number of advantages, including a smooth finish, denser concrete material, reduced wind pressure, and improved aesthetics.[5–8]

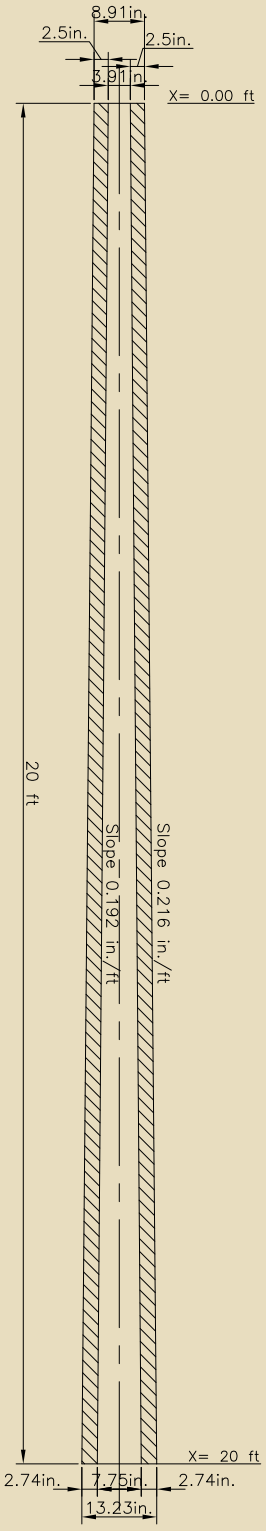

Figure 1. Specimen concrete dimensions. Note: All measurements not labeled are in inches. 1 in. = 25.4 mm; 1 ft = 0.305 m.

This paper presents the results of an experimental and analytical program on the strength and deflection behavior of spun concrete poles with CFRP reinforcement.

Experimental program

The main objective of the experimental program was to evaluate the flexural behavior of spun concrete poles reinforced with CFRP bars. Two sets of prototype pole specimens reinforced with CFRP bars were manufactured under normal precasting plant conditions. All specimens were identical except for the reinforcement scheme. The first set of specimens consisted of two poles, each reinforced with six CFRP longitudinal bars. One of the specimens used steel spiral reinforcement for confinement, and the second specimen used a CFRP grid. The second set of poles were each reinforced with twelve CFRP longitudinal bars but were otherwise identical to the first set of poles in geometry and confinement reinforcement.

Materials properties

The spun concrete test poles were produced using high-strength concrete. The 28-day compressive strength was 11,000 psi (76,000 kPa). The CFRP reinforcing bars are solid rods specially treated to enhance the bond to concrete. The no. 3 (10M) CFRP reinforcing bars had a cross-sectional area of 0.1010 in. (2.565 mm), a nominal diameter of 0.362 in.^{2} (234 mm^2), tensile strength of 300 ksi (2070 MPa), modulus of elasticity of 18,000 ksi (124,000 MPa), and an ultimate strain of 1.7%. The CFRP grid used for transverse confinement is a high-performance reinforcement made by bonding ultra-high-strength carbon tows with epoxy resin in a controlled factory environment. The grid has a designation of C50-2.9 × 2.9 and is composed of a square mesh of carbon strands spaced at 2.9 in. × 2.9 in. (72 mm × 72 mm). The longitudinal grid strength is 4.9 kip/ft (72 kN/m), and the transverse grid strength is 3.9 kip/ft (57 kN/m). The mesh strands have a tensile strength of 340 ksi (2340 MPa), a tensile modulus of elasticity of 34,000 ksi (234,000 MPa), an ultimate strain of 1.0%, a longitudinal cross-sectional area of 0.0036 in.^{2} (2.3 mm^2), and a transverse cross-sectional area of 0.00312 in.^{2} (2.0 mm^2). In some specimens, $^3/_{16}$-in.-diameter (5 mm) steel wire per ASTM A82[9] was used as spiral for the transverse reinforcement.

Specimen dimensions and reinforcement details

All test specimens were identical in geometry. Specimens were 20 ft (6.1 m) long with an outer diameter of 8.91 in. (226 mm) and 13.23 in. (336.0 mm) at the tip and butt ends, respectively, which provides an outside slope of 1.8% (0.216 in./ft). The inner diameters were 3.91 in. (99 mm) and 7.75 in. (191 mm) for the tip and butt ends, respectively, with an inside slope of 1.6% (0.192 in./ft). The wall thickness was 2.5 in. (63.5 mm) and 2.74 in. (69.6 mm) at the tip and butt ends, respectively. **Figure 1** shows the test specimens' dimensions. The size of the specimen was chosen to allow for easy transportation from

the production plant to the structural laboratory. The CFRP bars were $^{3}/_{8}$ in. (9 mm) in diameter and were distributed uniformly around the cross section. Steel spirals or CFRP grids were used for confinement (**Fig. 2** and **3**). The steel spirals had a wire diameter of $^{3}/_{16}$ in. (5 mm) with a pitch of 3.0 in. (75 mm) center to center and a concrete cover of 0.75 in. (19 mm). **Table 1** provides a summary of the geometry and reinforcement details for the test specimens. In Table 1, the first two digits of the specimen identification following the letter P represent the pole number, and the third and fourth digits represent the number of CFRP bars used. The letters SS indicate poles confined with steel spirals, and the letters CG indicate the poles confined with the carbon grid.

Test setup and procedure

Figure 4 shows the test setup. The pole specimen rested on two supports. The first support was located at the pole's butt end, and the second support, which served as the fulcrum, was located 3.0 ft (1 m) from the butt end. The distance to the fulcrum point was chosen to represent the typical foundation embedment length used in practice, which is

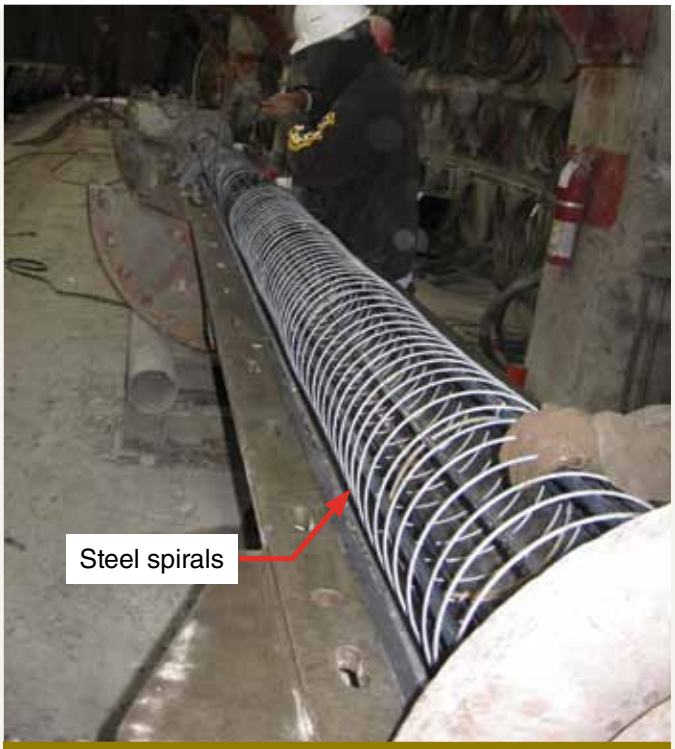

Figure 2. Pole confined with steel spiral.

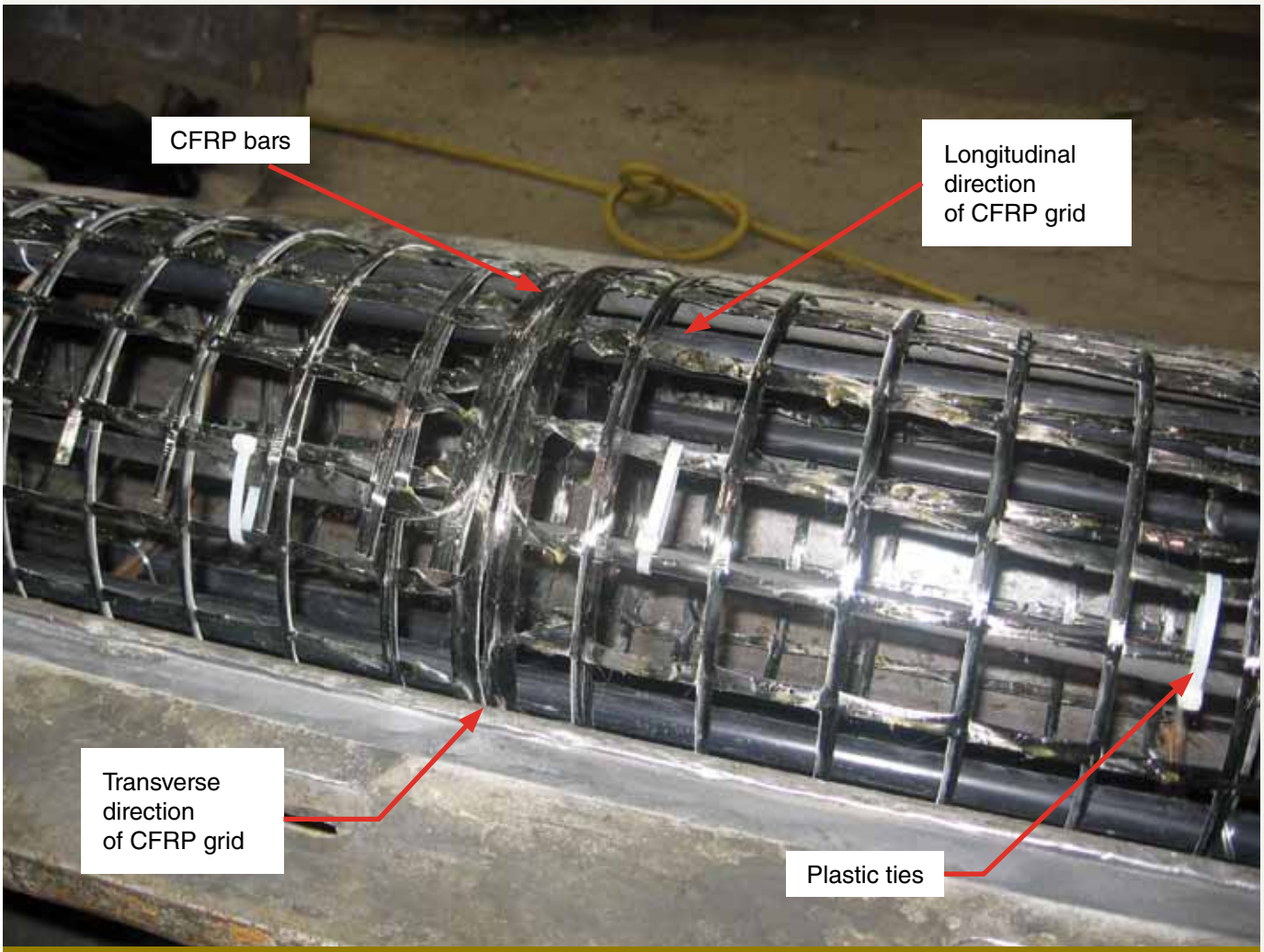

Figure 3. Pole confined with CFRP grid. Note: CFRP = carbon-fiber-reinforced polymer.

Table 1. Experimental program and CFRP specimen details

Specimen identification	Number of bars	Bar diameter, in.	Transverse reinforcement	Concrete cover, in.	Pole outer diameter, in.		Pole inner diameter, in.		Pole length, ft	Concrete strength, psi
					At tip	At butt	At tip	At butt		
P01-6SS	6	3/8	W2.9 at 3 in.	0.75	8.91	13.23	3.91	7.75	20	11,000
P02-6CG			C50-2.9 × 2.9							
P03-12SS	12	3/8	W2.9 at 3 in.	0.75	8.91	13.23	3.91	7.75	20	11,000
P04-12CG			C50-2.9 × 2.9							

Note: CFRP = carbon-fiber-reinforced polymer. 1 in. = 25.4 mm; 1 ft = 0.305 m; 1 psi = 6.895 kPa.

about 10% of the overall pole length plus 1 ft (0.30 m). The steel supports were designed and manufactured specifically to sustain the reactions from the load applied to the pole. The two supports were equipped with two semicircular collars on which the poles were placed and clamped (Fig. 4) to restrain them against lateral movement.

The load was applied at a distance of 1.0 ft (0.30 m) from the tip of the pole. The lever arm, measured to the centerline of the first restraining support (fulcrum point) was 16.0 ft (4.88 m). The load was applied using a manual chain hoist connected to a tension load cell and hooked to the trolley crane of the laboratory.

Two sets of strain gauges, each consisting of four gauges, were installed along the circumference of the pole at distances of 6 in. (150 mm) and 18 in. (450 mm) from the fulcrum support. For each set of strain gauges, two gauges were located at the vertical centerline of the cross section of the pole where the maximum compressive and tensile

Figure 4. Details of pole end supports.

Table 2. Summary of test results

Specimen identification	Number of bars	Cracking load, lb	Tip deflection at cracking, in.	Cracking strain, 10^{-6}	Failure load, lb	Corrected tip deflection at failure, in.	Concrete compressive failure strain, 10^{-4}	Maximum concrete compressive strain, 10^{-4}
P01-6SS	6	568	0.59	97	3790	25.84	32.06	35.58
P02-6CG		1025	1.54	170	4102	25.91	n.a.	24.96
P03-12SS	12	545	1.08	96	4247	20.465	n.a.	23.05
P04-12CG		904	0.92	106	5251	21.99	26.44	26.44

Note: n.a. = not applicable. 1 in. = 25.4 mm; 1 lb = 4.448 N.

stresses occur, and the other two gauges were located at the horizontal centerline (the neutral axis) of the cross section of the pole.

The tip deflection was recorded by two means. The first was a scale attached to the test frame near the tip of the pole, and the second was a tape connected to the pole. After the first cracking of the specimen, the crack width was measured at each load increment using crack comparators. The strain gauges and the load cell readings were recorded via a data acquisition system, and the data were transferred to a computer for analysis.

Two linear variable differential transformers (LVDTs) were installed adjacent to the supports of the test pole to record any movement that might occur at the supports. The readings would be used to correct the measured deflection at the tip of the pole.

The load was applied in increments of about 100 lb (444.8 N). There was a pause after each load increment to allow for reading deflections, inspecting for cracks, and observing any structural distress that might have occurred. Two test specimens were subjected to loading and unloading cycles to study the elastic and plastic deformation of the poles and inspect cracks after unloading. Pole P02-6CG was loaded up to 80% of the designed ultimate load, and the load was totally released. Then the pole was reloaded again up to failure. Pole P04-12CG was loaded up to 50% of the designed ultimate load, and the load was released and then reloaded up to 80% and released and then reloaded up to failure.

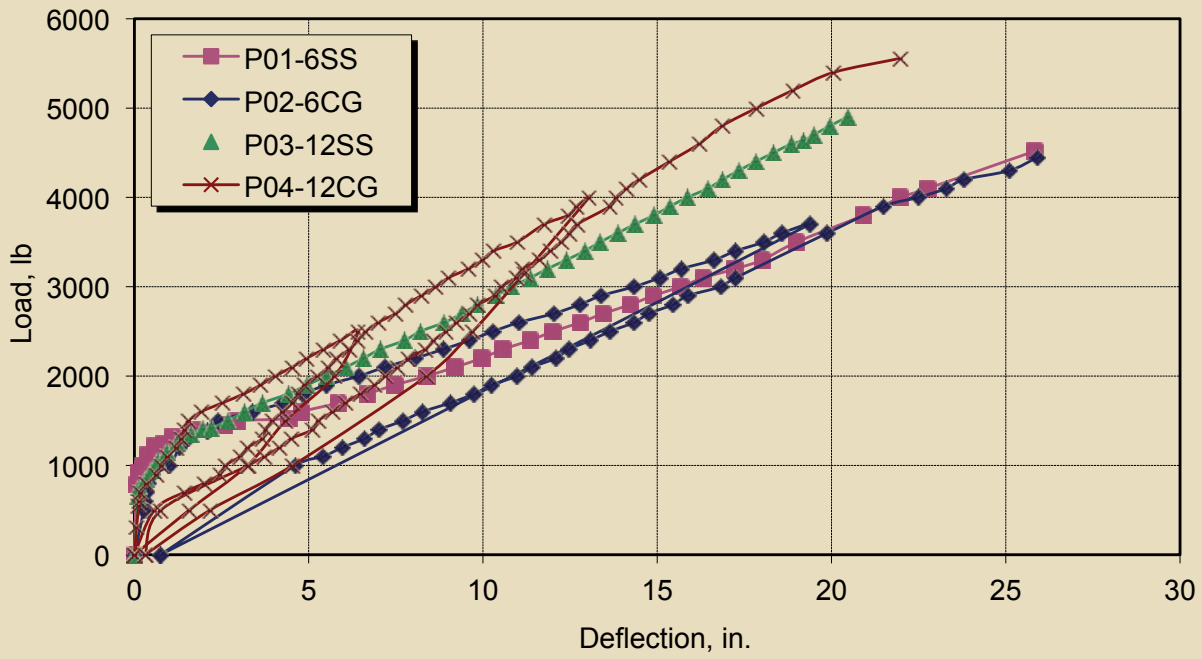

Figure 5. Load-deflection curve of the four specimens. Note: 1 in. = 25.4 mm; 1 lb = 4.448 N.

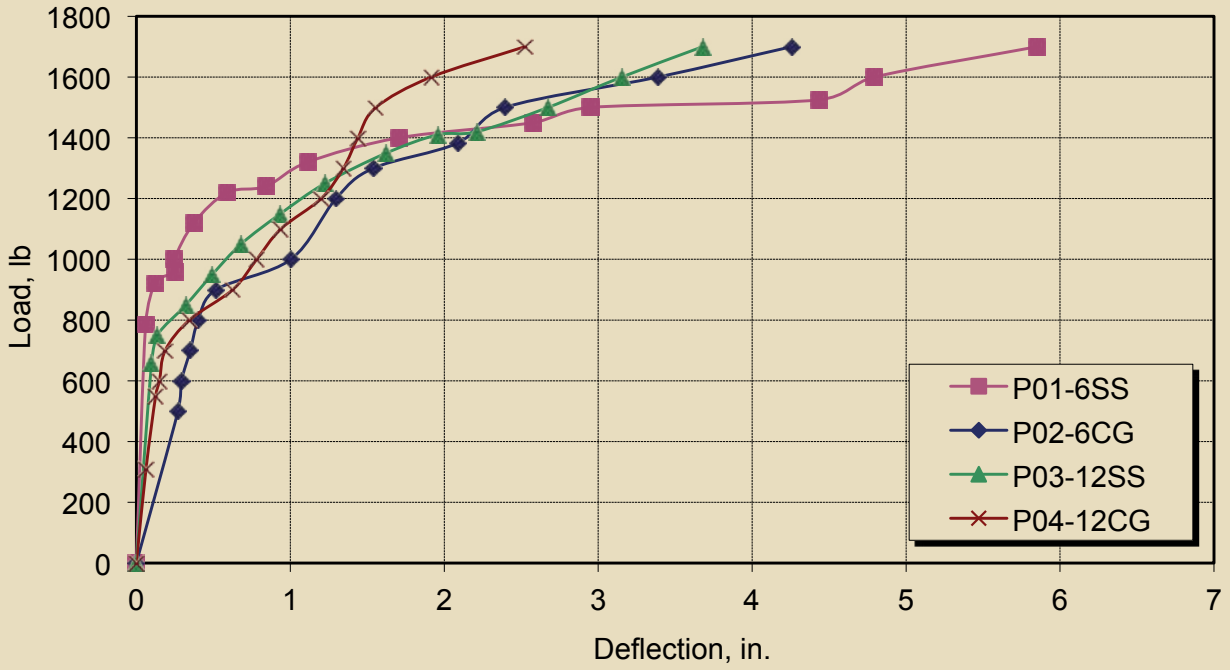

Figure 6. Load-deflection curve of the four specimens up to a load of 1700 lb. Note: 1 in. = 25.4 mm; 1 lb = 4.448 N.

Test results

Table 2 gives a summary of the test results. The poles reinforced with six CFRP bars provided higher deflection values at failure load (about 12% of the free length of the poles) than the pole reinforced with 12 CFRP bars (about 10% of the free length of the poles). The poles confined with the carbon grid failed at higher loads than those confined with steel spirals. The failure load of the poles confined with the carbon grid was higher than that of the poles confined with steel spirals by 8% and 24% for the poles reinforced with 6 CFRP bars and 12 CFRP bars, respectively. The reasons for these differences are explained later in this paper.

Deflection **Figure 5** shows the load-deflection curves of all specimens from zero loading to failure. **Figure 6** plots the load-deflection curves from zero loading up to a load of 1700 lb (7.56 kN). All specimens deflected linearly with load and had almost the same deflection values up to a load of about 750 lb (3.34 kN), which corresponds to the average cracking load of the poles. Following the cracking load and up to a load of 1500 lb (6.67 kN), the poles started to deflect nonlinearly with load, but the deflection curves still almost coincided with each other. In this nonlinear stage, cracks began to form in several locations along the pole length. At loads greater than 1500 lb, no more cracks formed. The load-deflection behavior became linear again, but the slope of the line was significantly smaller than the slope before cracking. The slope of this linear portion was different for the specimens. The poles reinforced with 12 CFRP bars had higher stiffness than the poles reinforced with 6 CFRP bars (Fig. 5). The poles confined with the carbon grid had higher stiffness than the poles confined with steel stirrups, which shows a contribution of the carbon grid to the increase in stiffness after cracking.

Failure mode Specimens P01-6SS and P03-12SS experienced compression failure at the fulcrum support, while specimens P02-6CG and P04-12CG experienced diagonal tension shear failure between supports combined with compression shear failure at the fulcrum support. For poles confined with steel spirals, diagonal shear cracks formed between the two supports prior to failure. At failure, the concrete crushed explosively in compression near the fulcrum support independent of the diagonal shear cracks (**Fig. 7**). For poles confined with the carbon grid, diagonal shear cracks formed between the two supports prior to failure. As the load increased, the diagonal shear cracks widened and extended to the top compression fibers of the pole and a sudden failure took place as this crack joined the crushed concrete zone (**Fig. 8**). The failure of these poles was also characterized by slippage of the CFRP bars at failure (**Fig. 9**). This slippage is due to the destruction of the bond between the longitudinal bars and the surrounding concrete in the support region, which frequently occurs in conjunction with the flexural shear failure mode.

After reaching the ultimate load and unloading the poles, pole P01-6SS underwent permanent cracking and deflection. This permanent cracking and deflection could be due to the low reinforcement ratio used in this pole. The lower reinforcement ratio results in higher strains and stresses in the reinforcement bars and consequently wider cracks.

Figure 7. Concrete crushing at failure for poles confined with steel spirals.

With the wide cracks and the difference between the modulus of elasticity of concrete and CFRP bars, the cracks were irrecoverable and the pole underwent permanent cracking and deflection. On the other hand, all of the cracks in pole P03-12SS were closed, leaving some hairline cracks, and the residual deflection recorded was low. This could be attributed to the number of bars used in this pole. With more bars, lower strains and stresses were transferred from the concrete to the reinforcement, resulting in narrower cracks that close on unloading.

Crack spacing **Figure 10** shows the crack pattern along the length of pole P01-6SS after reaching the ultimate load and unloading the pole. The residual crack width for this pole was 0.04 in. (1.0 mm), and the crack was located at 1 ft (0.3 m) from the fulcrum support toward the tip end of the pole on the tension side. Other residual cracks in this region were about 0.035 in. (0.89 mm) and were spaced at 4 in. (100 mm). Moving toward the middle of the pole up to 10 ft (3.0 m) from the butt end, the residual crack width decreased to an average of 0.02 in. (0.5 mm); however, the crack spacing ranged from 3 in. to 4 in. (75 mm to 100 mm). For the second half of the pole—10 ft (3.0 m) from the butt end up to 5 ft (1.5 m) from the tip end—the residual crack width measured an average of 0.007 in. (0.2 mm) with crack spacing of 6 in. (150 mm). There was no cracking observed for the rest of the pole. For pole P02-6CG, after reaching the ultimate load and unloading the pole, all of the cracks were closed, leaving only hairline cracks. Although there were not as many cracks as with pole P01-6SS, the cracks for pole P02-6CG were spaced every 4.0 in. (100 mm), from the fulcrum support on the tension side to 10 ft (3050 mm) from the butt end.

Figure 11 shows the crack pattern along the length of pole P03-12SS. All of the cracks left after unloading were hairline cracks that were hardly visible, and they were distributed at 4 in. (100 mm) from the fulcrum support to 10 ft (3.0 m) from the butt end. For the rest of the pole, no cracks were observed. The crack distribution for pole P04-12CG was similar to the crack distribution of pole P03-12SS.

From these observations, it can be concluded that the num-

Figure 8. Concrete failure for poles confined with carbon-fiber-reinforced polymer (CFRP) grid.

ber of reinforcing bars in the pole does not have a significant effect on the crack spacing.

Crack width **Figure 12** shows the crack width versus loading for pole P02-6CG at 2 ft (0.6 m) from the fulcrum support where the first crack was formed, and it also shows the crack width versus loading at 1 ft (0.305 m) from the fulcrum support for the poles reinforced with 12 CFRP bars. The crack widths for the pole reinforced with 6 CFRP bars were much wider than those for the poles reinforced with 12 CFRP bars. Also, for pole P02-6CG, the crack widths were significantly increased by loading and unloading, whereas there was no difference in the crack widths for pole P04-12CG when subjected to loading and unloading cycles. It was concluded that the number of bars significantly affects the crack widths of the poles.

Figure 12 also shows that the cracks for the pole P04-12CG confined with the CFRP grid are much narrower than for the pole P03-12SS confined with steel spirals. Confining the pole with CFRP grid means that the pole has CFRP strands in both circumferential and longitudinal directions. The CFRP strands in the longitudinal direction were spaced at 2.9 in. (72 mm) and had a small cross-sectional area. These properties resulted in a gradual transfer of the concrete tensile stress to the reinforcing bars, significantly reducing the crack widths of the pole.

The significant reduction in the crack widths for poles confined with CFRP grid compared with poles confined with steel spirals resulted in an increase in the area of concrete subjected to compression. The tensile force in the CFRP bars also increased, balancing the compression force and increasing the ultimate moment capacity. Table 2 shows the differences in the ultimate capacities of the poles confined with the CFRP grid and those confined with steel spirals.

Analytical study

Theoretical studies were performed prior to testing to predict the behavior of the spun concrete poles reinforced with CFRP and were compared with the experimental results. Design equations available in the literature and de-

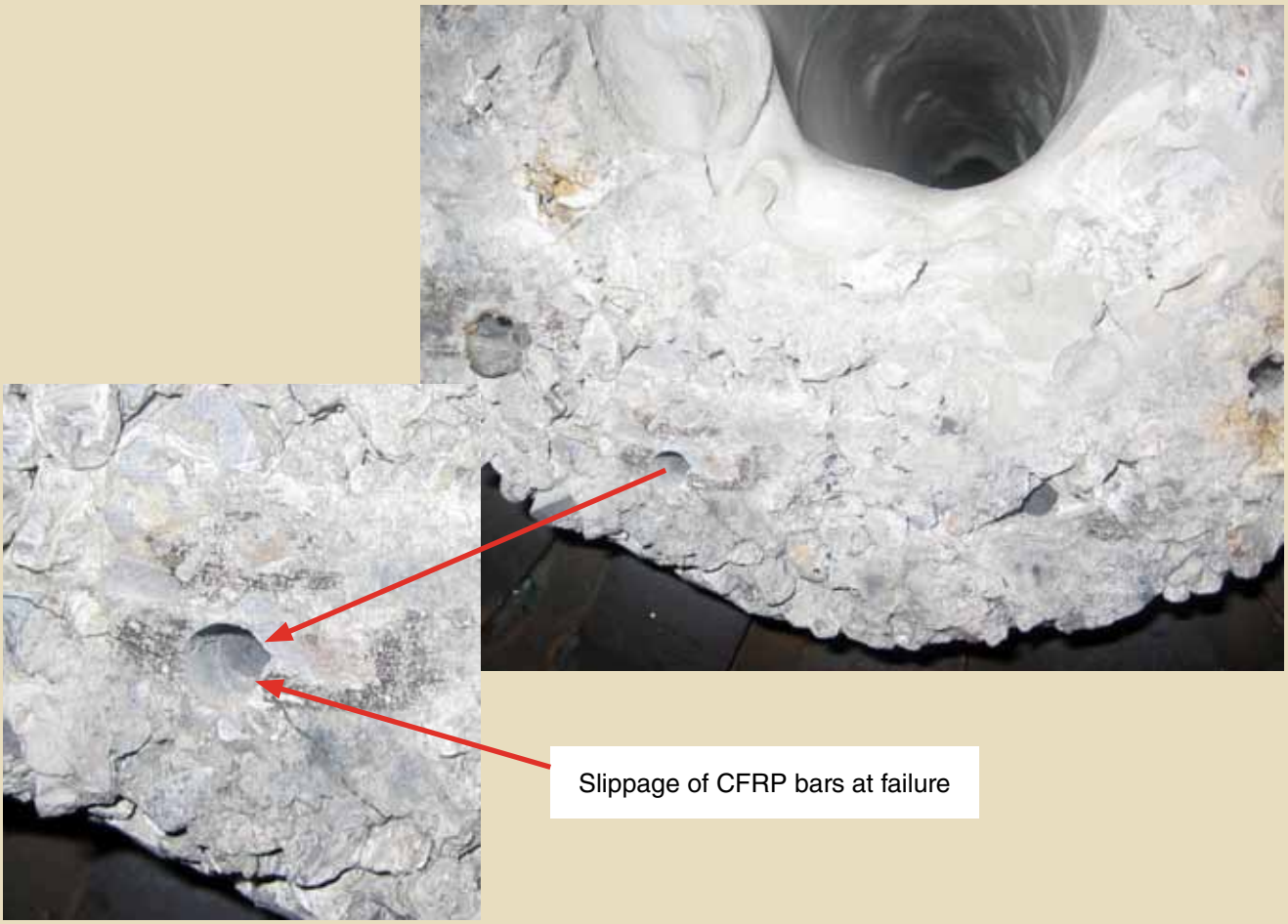

Figure 9. Slippage of CFRP bars at failure of poles confined with CFRP grid. Note: CFRP = carbon-fiber-reinforced polymer.

sign guidelines for concrete poles and concrete structures reinforced with CFRP[10–13] were evaluated and modified to estimate the flexural capacity, short-term deflection, and crack widths of the spun pole test specimens.

Ultimate moment capacity

The ultimate moment capacity M_u of the poles was determined based on strain compatibility and the internal force equilibrium (**Fig. 13**) as follows:

$$M_u = , = \sum_{i=1}^{n} e_i A_{fi} f_{fei} + C_c\left(c - Kc\right)$$

$e_i = d_i - c$

$f_{fei} \leq f_{fu}$

where

e_i = distance of the i^{th} reinforcement from the neutral axis

A_{fi} = area of the i^{th} reinforcement

f_{fei} = stress of the i^{th} reinforcement

C_c = compression force

c = distance of the neutral axis from the extreme compression fiber of the pole

Kc = position of the centroid of the stress block

d_i = distance of the i^{th} reinforcement from the extreme compression fiber

f_{fu} = ultimate strength of the CFRP bars

The distance c of the neutral axis from the extreme compression fiber of the pole is calculated by trial and error to balance the compression and tension forces acting on the cross section. A spreadsheet facilitated the analysis and design process.

Unlike traditional steel reinforcement, CFRP is a linearly elastic material up to failure and does not have a yield point, which implies a sudden failure once the CFRP bar reaches its ultimate strength.

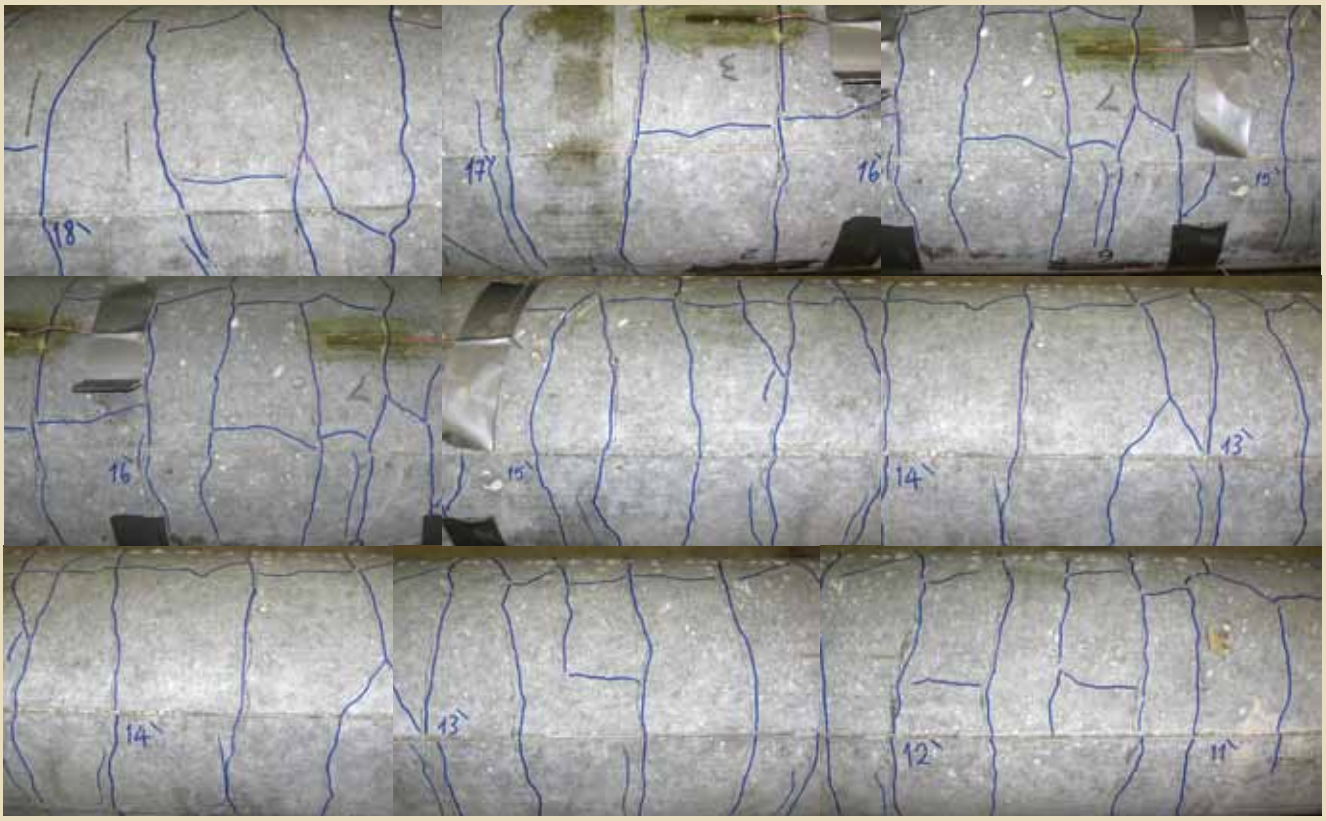

Figure 10. Cracking pattern for pole P01-6SS.

Cracking moment capacity

Cracking starts when the tensile stress in the extreme fiber of the concrete reaches its modulus of rupture. The cracking moment M_{cr} can be computed by elastic theory to predict the behavior of poles and is calculated, as proposed by American Concrete Institute's (ACI's) *Building Code Requirements for Structural Concrete (ACI 318-08) and Commentary (ACI 318R-08)*,[10] using the following relationships:

$$M_{cr} = \frac{f_r I_g}{y_t}$$

$$f_r = 7.5\sqrt{f'_c}$$

where

f_r = modulus of rupture of concrete

I_g = gross moment of inertia of the section

y_t = distance from the centroidal axis to the extreme tensile fiber of the section

f'_c = cylinder compressive strength of concrete at 28 days

Deflection

Theoretical deflection Δ calculations were performed using the virtual work method.

$$\Delta = \int_0^L \frac{Mx}{E_c I} dx$$

where

L = length of the pole

M = applied moment

x = distance from the support

E_c = modulus of elasticity of concrete

I = moment of inertia of the cross section

Before cracking of the concrete section, the gross moment of inertia I_g is used to calculate the deflection; after cracking, the effective moment of inertia I_e is used. Concrete poles are tapered structures, so their moment of inertia is variable along the pole length.

Previous studies[14–16] showed that Branson's[17] equation for calculating the effective moment of inertia of concrete for

Figure 11. Cracking pattern for pole P03-12SS.

structures subject to bending underestimates the deflection of concrete structures reinforced with fiber-reinforced polymer (FRP) bars and proposed several modifications to account for the difference in behavior between concrete structures reinforced with steel and those reinforced with FRP. Accordingly, ACI's *Guide for the Design and Construction of Concrete Reinforced with FRP Bars (ACI 440.1R-03)*[11] introduced a reduction coefficient β_d to be added to the first term of Branson's equation as follows:

$$I_e = \left(\frac{M_{cr}}{M_a}\right)^3 \beta_d I_g + \left[1 - \left(\frac{M_{cr}}{M_a}\right)^3\right] I_{cr} \leq I_g$$

$$\beta_d = \alpha_b \left(\frac{E_f}{E_s} + 1\right)$$

where

M_a = maximum applied moment

I_{cr} = cracking moment of inertia

α_b = bond-dependent coefficient that was recommended to be equal to 0.5 until more data became available

E_f = modulus of elasticity of FRP bars

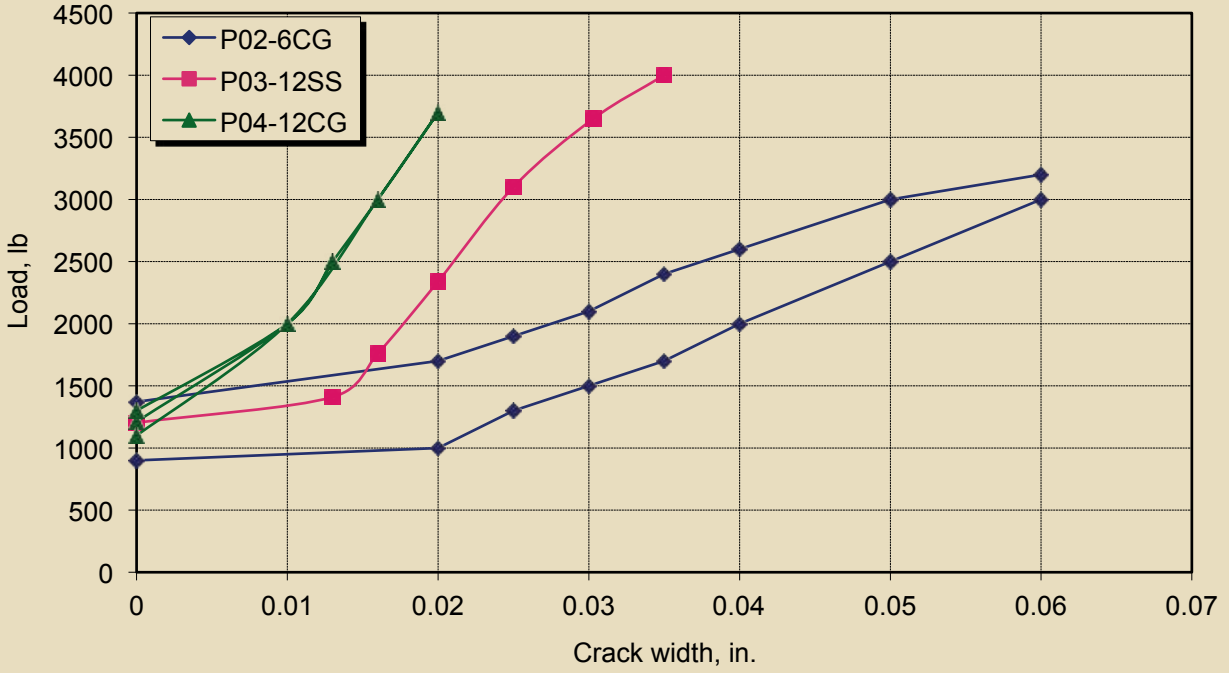

Figure 12. Crack width versus loading. Note: 1 in. = 25.4 mm; 1 lb = 4.448 N.

E_s = modulus of elasticity of steel bars

The cracking moment of inertia for circular hollow sections with reinforcing bars distributed around the entire cross section is calculated as follows:

$$I_{cr} = I_{A_a} + \sum_{i=1}^{n} n_f A_{f_i} e_i^2$$

where

I_{A_a} = moment of inertia of annulus calculated at the neutral axis

n_f = modular ratio between CFRP and concrete

Upon ACI Committee 440's recommendation to develop more experimental data to comprehensively evaluate the

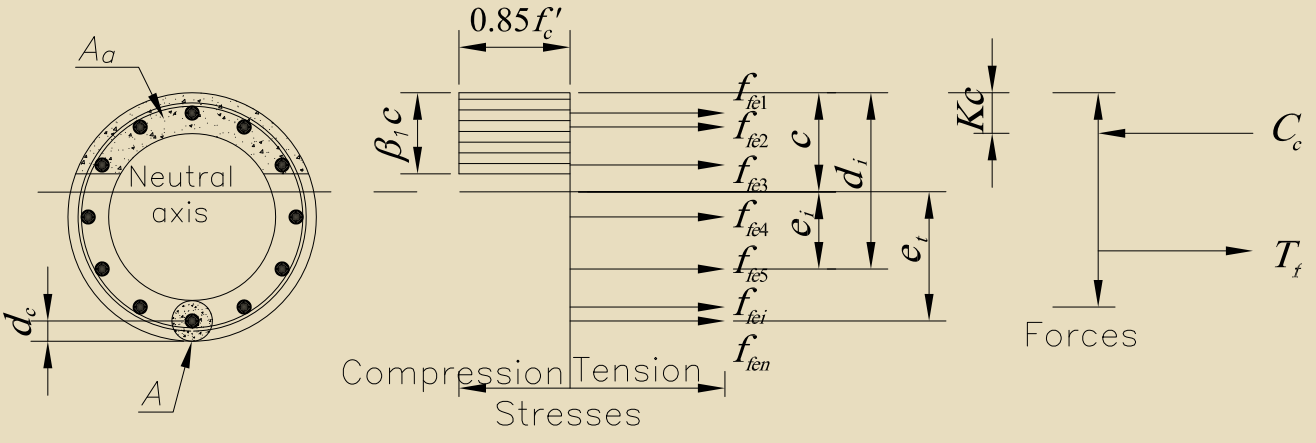

Figure 13. Assumed stress distribution and crack width parameter for pole specimens. Note: A = effective tension area of concrete with the same centroid as the tensile reinforcement farthest from neutral axis; A_a = area of the annulus; c = location of the neutral axis measured from the extreme compression fiber of the pole; C_c = compression force; d_c = distance from the centroid of the effective tension area of concrete to the extreme tensile fiber of the cross section; d_i = distance of the i^{th} reinforcement from the extreme compression fiber; e_i = distance of the i^{th} reinforcement to the neutral axis; f'_c = cylinder compressive strength of concrete at 28 days; f_{fei} = stress in the i^{th} reinforcement; f_{fen} = stress in extreme tensile reinforcement; K_c = position of the centroid of the stress block; T_f = tension force; β_1 = ratio of the depth of the equivalent rectangular stress block to the depth of the neutral axis.

value of the bond-dependent coefficient, Yost et al.[18] conducted a research study that focused mainly on evaluating the accuracy of I_e. Yost et al. claimed that the accuracy of the ACI 440.1R-03 equation for the calculation of the effective moment of inertia for concrete structures reinforced with FRP bars relied primarily on the reinforcement ratio of the member.[19] Yost et al. proposed a new formula for the bond-dependent coefficient α_b as follows:

$$\alpha_b = 0.064\left(\frac{\rho}{\rho_b}\right) + 0.13$$

where

r = reinforcement ratio

ρ_b = balanced reinforcement ratio

For circular hollow sections, these ratios are calculated as follows:

$$\rho = \frac{A_f}{A_g}$$

$$\rho_b = \frac{0.85 f_c' \beta_1 A_a}{f_{fu} A_g}$$

where

A_f = cross-sectional area of the FRP reinforcement

A_g = gross area of the cross section

β_1 = ratio of the depth of the equivalent rectangular stress block to the depth of the neutral axis

A_a = area of annulus

A_{fu} = ultimate tensile strength of the FRP reinforcement

ACI's *Guide for the Design and Construction of Concrete Reinforced with FRP Bars* (ACI 440.1R-06)[12] also proposed revisions to the deflection equation in ACI 440.1R-03. The reduction coefficient β_d was modified. The key variable in the equation was changed from the modulus of elasticity of FRP reinforcement to the relative reinforcement ratio,[19] as shown in the following equation:

$$\beta_d = \frac{1}{5}\left(\frac{\rho}{\rho_b}\right) \le 1.0$$

Bischoff and Scanlon[20] concluded that Branson's equation underestimates the deflection of concrete members reinforced with FRP because the ratio I_g/I_{cr} is typically greater than 3. Therefore, they proposed a new equation to calculate the effective moment of inertia based on a weighted average of flexibility rather than stiffness. The proposed equation is as follows:

$$I_e = \frac{I_{cr}}{\left[1 - \eta\left(\frac{M_{cr}}{M_a}\right)^2\right]} \le I_g$$

$$\eta = 1 - \frac{I_{cr}}{I_g}$$

where

η = moment of inertia coefficient

In this study, the deflection of spun concrete poles reinforced with CFRP bars was theoretically calculated using the virtual work method and literature equations.[12,20] The results from the analytical study were compared with test data from the experimental program.

Crack width

The following equation from ACI 440.1R-03 was used to calculate the crack width w of spun concrete poles reinforced with CFRP.

$$w = \frac{2200}{E_f} \beta k_b f_{fei} \sqrt[3]{d_c A}$$

$$\beta = \frac{e_t}{e_i}$$

β = ratio between the distance of the i^{th} reinforcement to the neutral axis and the distance of the extreme reinforcement bar to the neutral axis

k_b = bond coefficient, assumed to be 1.0 for this study

d_c = distance from the centroid of the effective tension area of concrete to the extreme tensile fiber of the cross section

A = effective tension area of concrete defined as the area of concrete that has the same centroid as that of the tensile reinforcement farthest from the neutral axis

e_t = distance from the neutral axis to the extreme tensile reinforcement bar

Table 3. Theoretical and experimental cracking moments at 6 in. from the fulcrum support

Specimen identification	Cracking moment		Difference, %	Ultimate moment		Difference, %
	Theoretical, kip-ft	Experimental, kip-ft		Theoretical, kip-ft	Experimental, kip-ft	
P01-6SS	11.46	9.09	+26	59.48	60.64	-2
P02-6CG	11.46	16.40	-30	59.48	65.63	-9
P03-12SS	11.46	8.72	+31	74.25	67.95	+9
P04-12CG	11.46	14.46	-21	74.25	84.02	-12
Average	11.46	12.17	-6	n.a.	n.a.	n.a.

Note: n.a. = not applicable. 1 in. = 25.4 mm; 1 kip-ft = 1.36 kN-m.

A bond coefficient of 1.0 means that the CFRP bars have the same bond strength as the traditional steel reinforcement. A higher value for the bond coefficient means higher bond strength. A smaller value means lower bond strength.

The equation was developed for a rectangular concrete section with a single layer of reinforcement. However, spun concrete poles are round and the reinforcement is aligned around the cross section. Therefore, the definition of the effective tension area of concrete A was modified to account for the shape difference and reinforcement alignment between rectangular and circular concrete sections. In rectangular concrete sections with a single layer of reinforcement, the effective tension area of concrete A is the area of concrete that has the same centroid as that of tensile reinforcement divided by the number of bars. In this study, the effective tension area of concrete A was defined as the area of concrete that has the same centroid as that of the tensile reinforcement farthest from the neutral axis (Fig. 13).

Results and discussion

Cracking and ultimate moments

Table 3 shows the theoretical and experimental cracking moments of the poles. Because the cracking moment depends mainly on the modulus of rupture of the concrete and the reinforcement ratio has a small effect, the average cracking moment of the four poles was compared with the theoretical cracking moment. The test yielded an average cracking moment of 12.17 kip-ft (16.50 kN-m) versus the theoretical cracking moment of 11.46 kip-ft (15.54 kN-m). The difference between the theoretical and experimental values is only 6%, which indicates comparable results. Table 3 also shows the theoretical and experimental ultimate moments of the poles. The theoretical ultimate moment capacity was close to the experimental ultimate moment for pole P01-6SS with only 2% difference. For pole P03-12SS, the theoretical ultimate moment capacity was higher than the experimental ultimate moment by 9%. For the other two poles confined with the CFRP grid (P02-6CG and P04-12CG), the experimental ultimate moment capacities were higher than the theoretical by 9% and 12%, respectively. This increase may be attributed to the confinement provided by the CFRP grid as well as the strands of the CFRP grid in the longitudinal direction of the pole, which will contribute to the increase in the ultimate capacity of the poles.

Deflection

Figures 14 and **15** and **Table 4** show a comparison between the load-deflection data obtained from the experimental program and those theoretically developed using the literature equations.[12,20] The ACI 440.1R-06 equation underestimates the deflection of the poles reinforced with CFRP bars by as much as 45%. The Bischoff and Scanlon[20] equation underestimates the deflection of the poles reinforced with CFRP bars by 10%.

The literature equations[12,20] for calculating the effective moment of inertia for concrete structures reinforced with FRP bars may be revised for spun concrete poles reinforced with CFRP bars for a better deflection estimate.

Figures 16 and **17** compare the experimental deflection after cracking with the deflection calculated using the ACI 440.1R-06 equation and Bischoff and Scanlon[20] equation, respectively. A trend line was generated for both figures.

These figures show that the calculated deflection values using the literature equations are about 0.9 times the experimental values. The constant of 0.90 is similar to the reduction factor proposed by Benmokrane et al.,[14] where they multiplied the reduction factor by the cracking moment of inertia to obtain good correlation with experimental results. In a similar fashion, the constant of 0.90 obtained from Fig. 16 and 17 was multiplied by the cracking moment of inertia in the literature equations[12,20] to modify the equations for round cross sections as follows:

$$I_e = \left(\frac{M_{cr}}{M_a}\right)^3 \beta_d I_g + \alpha\left[1 - \left(\frac{M_{cr}}{M_a}\right)^3\right] I_{cr} \le I_g \qquad \text{Eq. (1)}$$

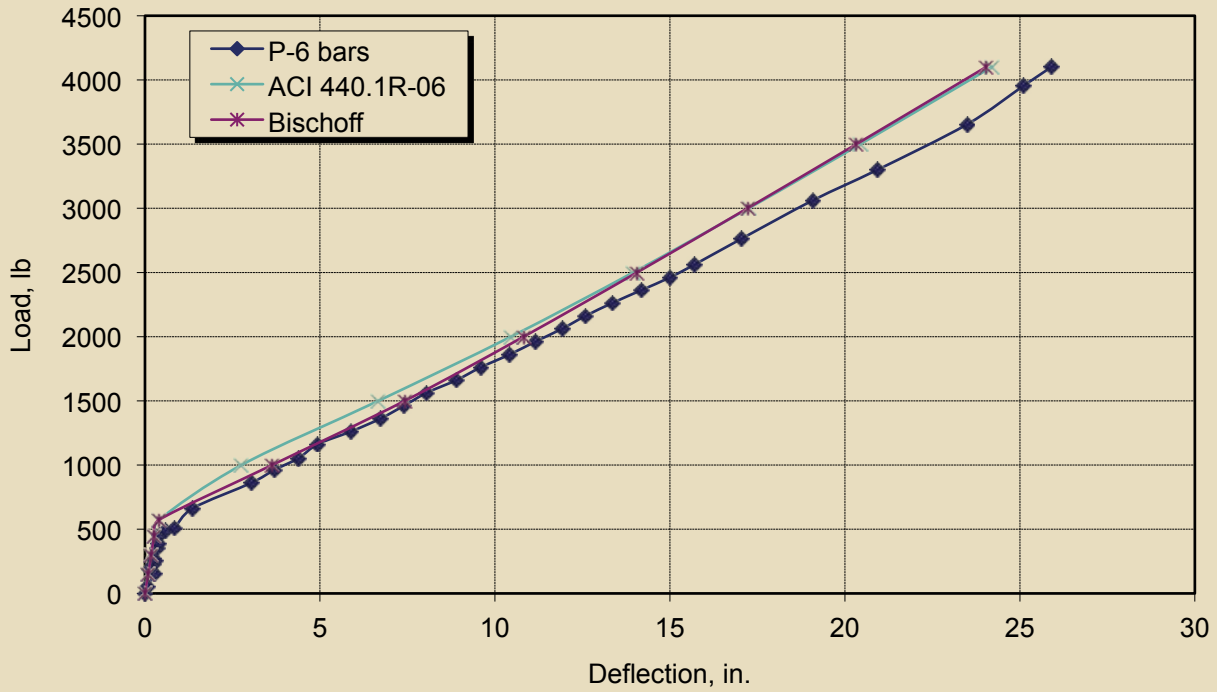

Figure 14. Load-deflection curve for the poles reinforced with six carbon-fiber-reinforced polymer (CFRP) bars. Note: 1 in. = 25.4 mm; 1 lb = 4.448 N.

$$\left.\begin{aligned} I_e &= \frac{\alpha I_{cr}}{\left[1-\eta\left(\frac{M_{cr}}{M_a}\right)^2\right]} \le I_g \\ \eta &= 1-\frac{\alpha I_{cr}}{I_g} \end{aligned}\right\} \quad \text{Eq. (2)}$$

where

α = reduction factor
= 0.90

This factor is attributed to differences in shape and reinforcement alignment between rectangular and circular concrete sections.

Figures 18 and **19** and **Table 5** compare the load-deflection curves obtained from the experimental results with those developed using the modified expressions. The deflection calculated using Eq. (1) underestimates the deflection of the poles under service loads, with no significant difference from the ACI 440.1R-06 proposed equation. At failure, the estimated deflection is overestimated by 4% for the poles reinforced with six CFRP bars and 1% for the poles reinforced with 12 CFRP bars. The load-deflection curve plotted using Eq. (2) estimated the deflection of the poles reinforced with CFRP bars within 3% on the conservative side. Therefore, it was concluded that Eq. (2) should be used for calculating deflections of poles reinforced with CFRP bars under service and ultimate loads.

Crack width

Table 6 shows the maximum crack width measured during the test compared with that calculated using the ACI 440.1R-03 equation. There is a significant difference between the test and calculated values for all of the poles except P03-12SS. For pole P01-6SS, the crack width was measured after reaching ultimate load and unloading the pole and moving it from the test frame, so this crack width does not represent the actual crack width during the test. For pole P02-6CG, the crack width was calculated at several load intervals that correspond to the experimental data recorded. At 70% of ultimate load, the equation used to calculate the crack width underestimates the crack width of the pole by about 15%; however, **Fig. 20** shows that at lower loads the calculated crack width is comparable to that measured during the test.

Figure 21 shows the load-crack width curve for the poles reinforced with 12 CFRP bars. For pole P03-12SS, the ACI 440.1R-03 equation correlated well with the experimental results, especially for higher loads. For lower loads, the correlation was not as good, unlike pole P02-6CG. For pole P04-12CG, the measured crack width during loading was significantly different from the measured crack width of pole P03-12SS and the theoretical calculations.

From this discussion, it could be concluded that using the ACI 440.1R-03 equation to estimate the crack width of spun concrete poles reinforced with CFRP bars will give misleading results. Additional testing is necessary to come up with a suitable formula that can be used to calculate the crack

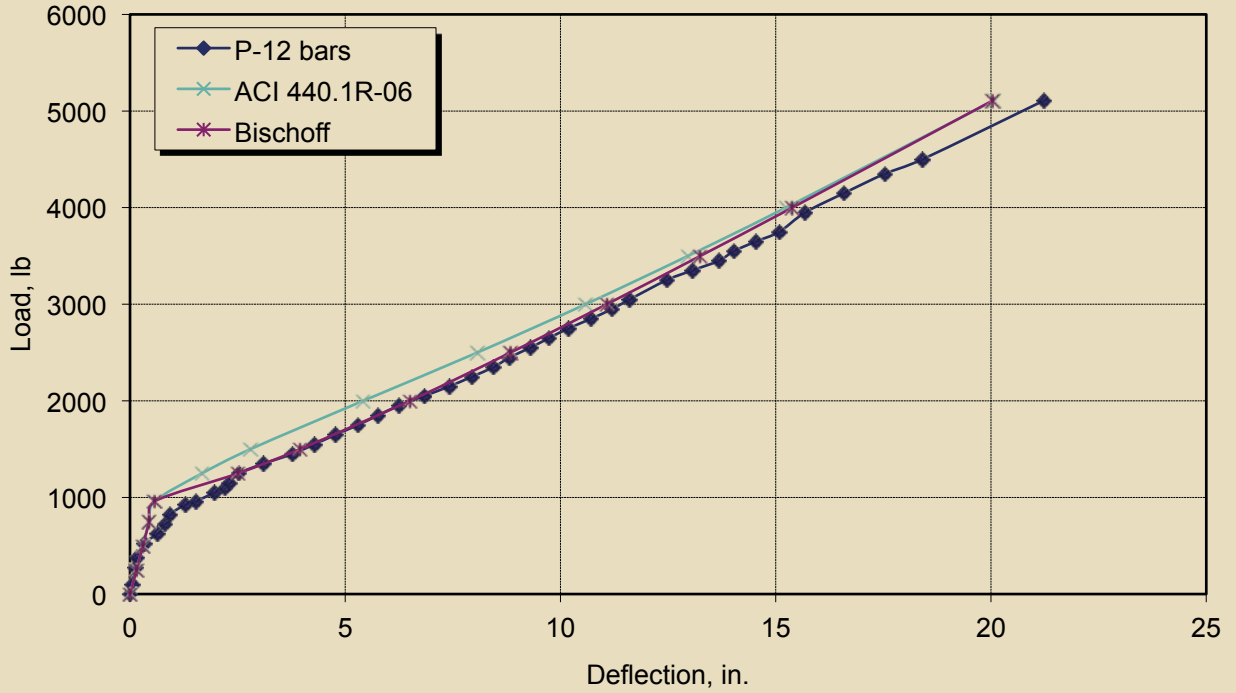

Figure 15. Load-deflection curve for the poles reinforced with 12 carbon-fiber-reinforced polymer (CFRP) bars. Note: 1 in. = 25.4 mm; 1 lb = 4.448 N.

Table 4. Experimental deflections versus ACI 440.1R-06 and Bischoff and Scanlon equation prediction deflections after pole cracking

Pole number	Load, lb	Experimental deflection, in.	ACI 440.1R-06 deflection, in.	Difference, %	Bischoff and Scanlon deflection, in.	Difference, %
P-6 bars	1000	4.39	2.76	37	3.63	17
	1500	8.04	6.67	17	7.42	8
	2000	11.92	10.46	12	10.82	9
	2500	15.70	13.95	11	14.06	10
	3000	19.08	17.25	10	17.22	10
	3500	22.21	20.44	8	20.33	8
	4102	25.91	24.20	7	24.04	7
P-12 bars	1250	3.10	1.68	46	2.51	19
	1500	4.53	2.80	38	3.95	13
	2000	7.13	5.42	24	6.50	9
	2500	9.52	8.07	15	8.84	7
	3000	12.04	10.58	12	11.07	8
	3500	14.28	12.96	9	13.25	7
	4000	16.58	15.24	8	15.38	7
	5108	22.00	20.06	9	20.04	9

Note: 1 in. = 25.4 mm; 1 lb = 4.448 N.

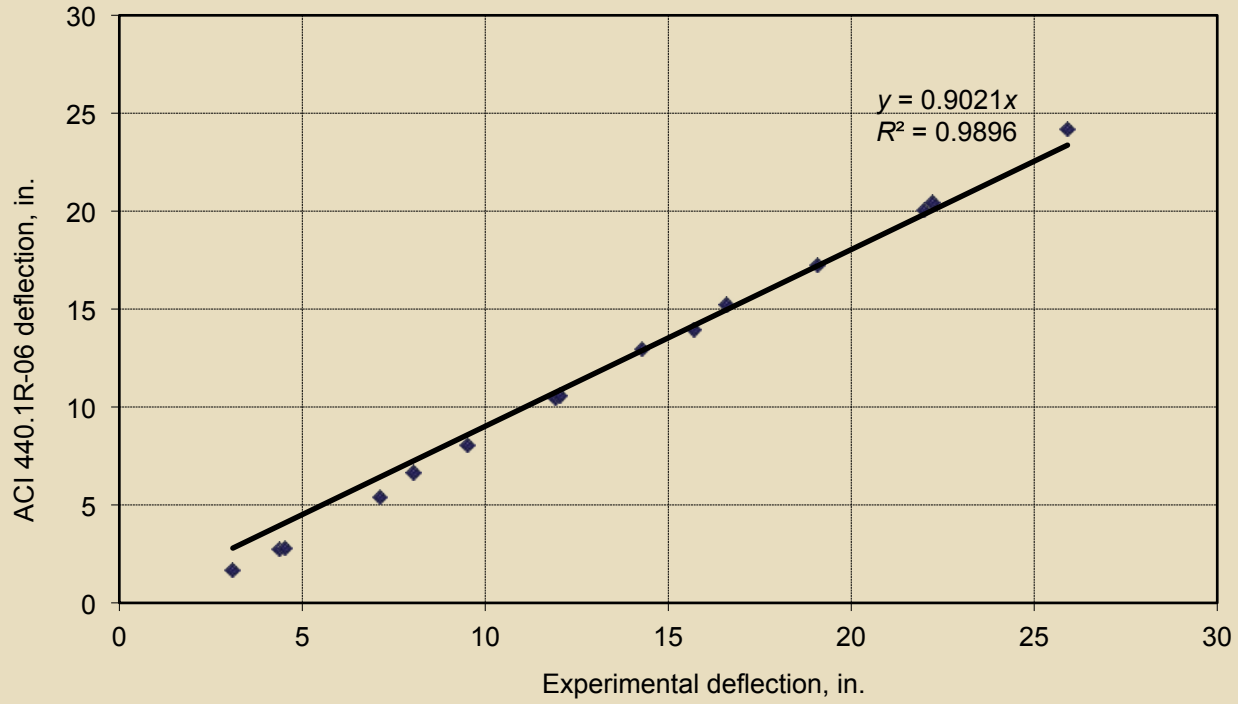

Figure 16. Experimental versus ACI 440.1R-06 deflection for poles reinforced with carbon-fiber-reinforced polymer (CFRP) bars. Note: 1 in. = 25.4 mm.

width of spun concrete poles reinforced with CFRP bars.

Conclusion

The conclusions drawn from this study can be summarized as follows:

- Concrete poles reinforced with CFRP bars showed satisfactory flexural behavior. Ductility was demonstrated by deflections of about 12% of the free length

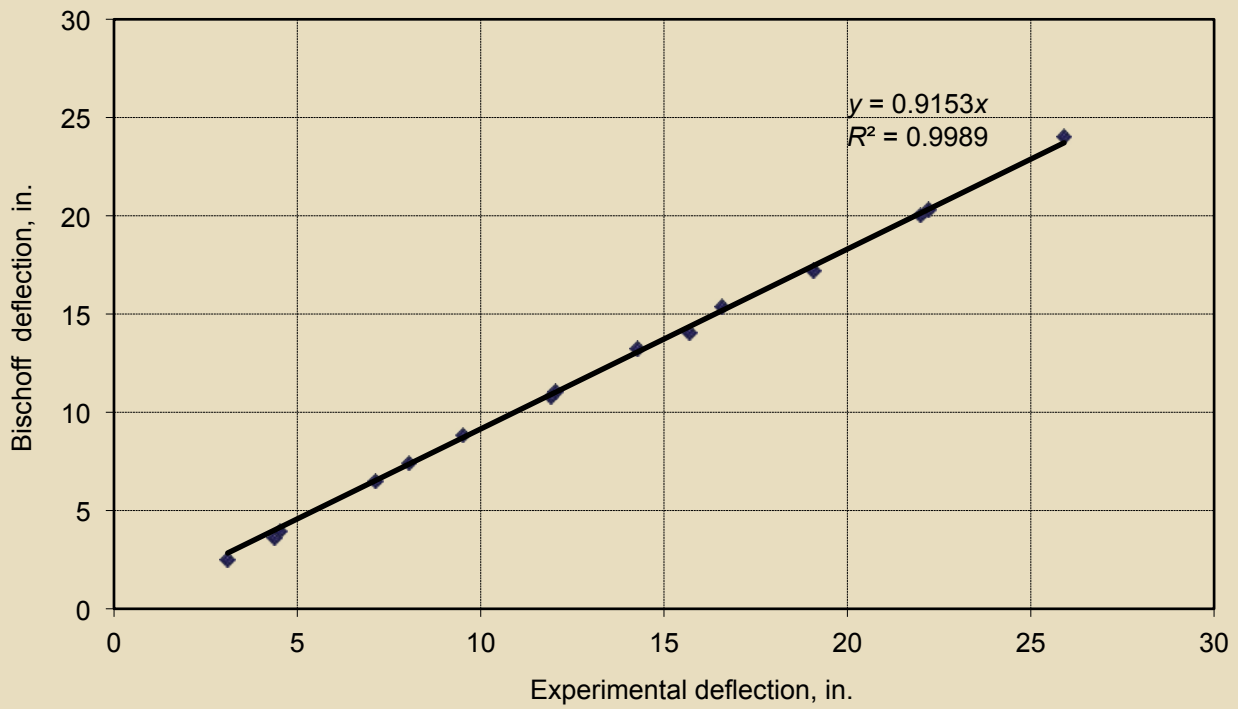

Figure 17. Experimental versus Bischoff deflection for poles reinforced with carbon-fiber-reinforced polymer (CFRP) bars. Note: 1 in. = 25.4 mm.

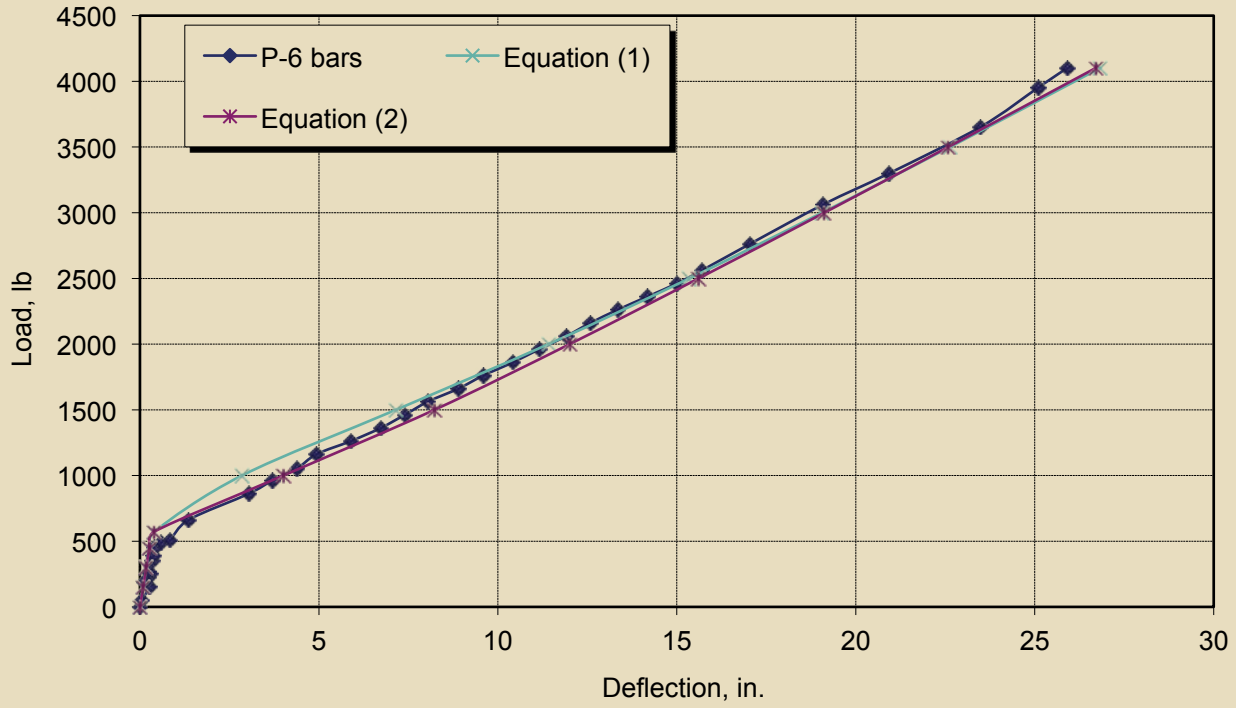

Figure 18. Modified load-deflection curve for the poles reinforced with 6 carbon-fiber-reinforced polymer (CFRP) bars. Note: 1 in. = 25.4 mm; 1 lb = 4.448 N.

of the pole prior to failure.

- The ultimate moment capacity of spun concrete pole cross sections reinforced with CFRP bars calculated using the proposed equations compared well with the experimental results.
- The number of reinforcing bars in the pole did not have a significant effect on crack spacing.

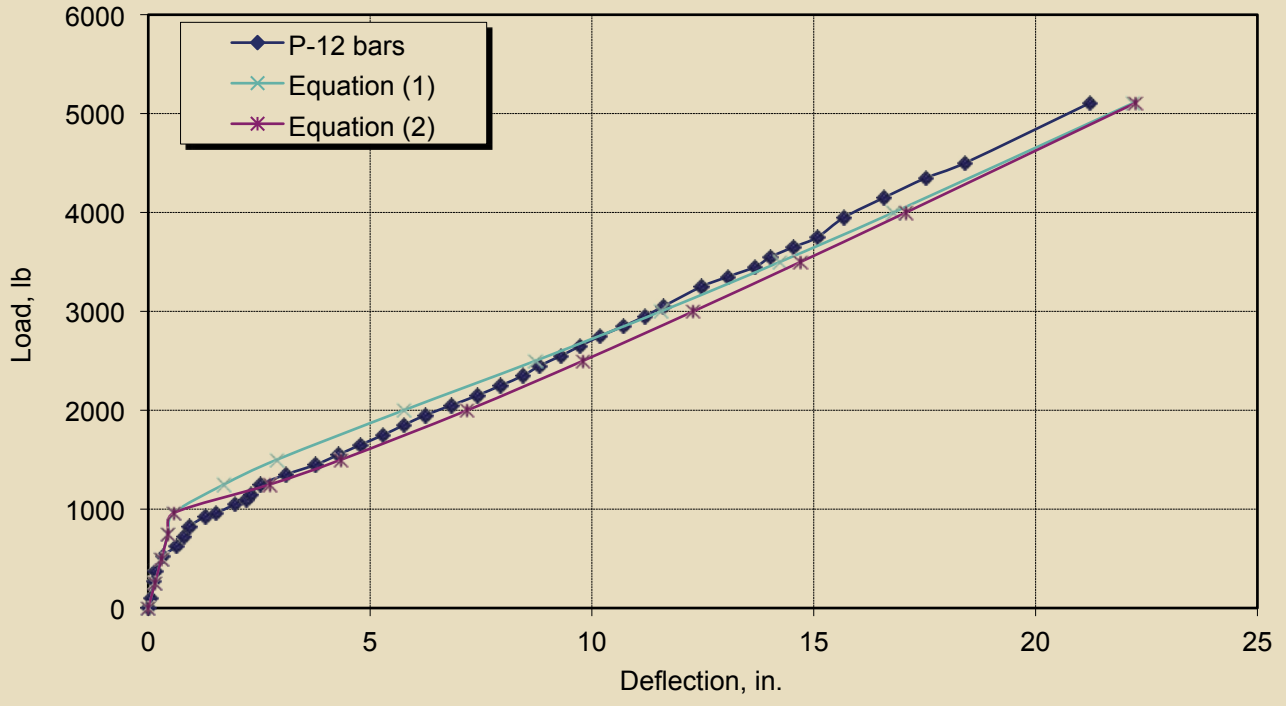

Figure 19. Modified load-deflection curve for the poles reinforced with 12 carbon-fiber-reinforced polymer (CFRP) bars. Note: 1 in. = 25.4 mm; 1 lb = 4.448 N.

Table 5. Experimental deflections versus Eq. (1) and (2) calculated deflections after pole cracking

Pole number	Load, lb	Experimental deflection, in.	Eq. (1) deflection, in.	Difference, %	Eq. (2) deflection, in.	Difference, %
P-6 bars	1000	4.39	2.85	35	4.01	9
	1500	8.04	7.15	11	8.23	-2
	2000	11.92	11.42	4	12.01	-1
	2500	15.70	15.35	2	15.61	1
	3000	19.08	19.06	0	19.12	0
	3500	22.21	22.63	-2	22.58	-2
	4102	25.91	26.83	-4	26.71	-3
P-12 bars	1250	3.10	1.71	45	2.74	12
	1500	4.53	2.90	36	4.35	4
	2000	7.13	5.76	19	7.19	-1
	2500	9.52	8.73	8	9.80	-3
	3000	12.04	11.56	4	12.28	-2
	3500	14.28	14.24	0	14.70	-3
	4000	16.58	16.80	-1	17.08	-3
	5108	22.00	22.21	-1	22.25	-1

Note: 1 in. = 25.4 mm; 1 lb = 4.448 N.

Table 6. Theoretical and experimental maximum crack width

Specimen identification	Load, lb	Portion of ultimate load, %	Crack width, mil	
			Experimental	Theoretical
P01-6SS	After unloading	n.a.	40	50
P02-6CG	2854	70	60	50
P03-12SS	3342	77	35	35
P04-12CG	3393	65	20	36

Note: n.a. = not applicable. 1 mil = 0.0254 mm; 1 lb = 4.448 N.

- The number of reinforcing bars in a pole significantly affects crack width. The crack widths of the poles reinforced with six CFRP bars were much greater than those for the poles reinforced with 12 CFRP bars. Also, the crack widths were significantly increased by loading and unloading for poles reinforced with six CFRP bars, whereas there was no difference in the crack widths for poles reinforced with 12 CFRP bars and subjected to loading and unloading cycles.
- Confining the poles with CFRP grid significantly decreased crack widths. In poles with the same reinforcement ratios, crack widths for the poles confined with the CFRP grid were about 40% less prior to failure compared with the poles confined with steel spirals.
- Confining the poles with CFRP grid affected their failure mode. The poles reinforced with CFRP grid failed in flexural compression shear mode between the supports, with bars failing through bond. The poles confined with steel spirals underwent compression failure at the support due to flexure with comparable failure loads.
- Literature equations[12,20] used to calculate the effective moment of inertia of concrete structures reinforced with FRP need to be revised to account for members with round cross sections.
- Based on the correlation between experimental and theoretical results, modified expressions for the ef-

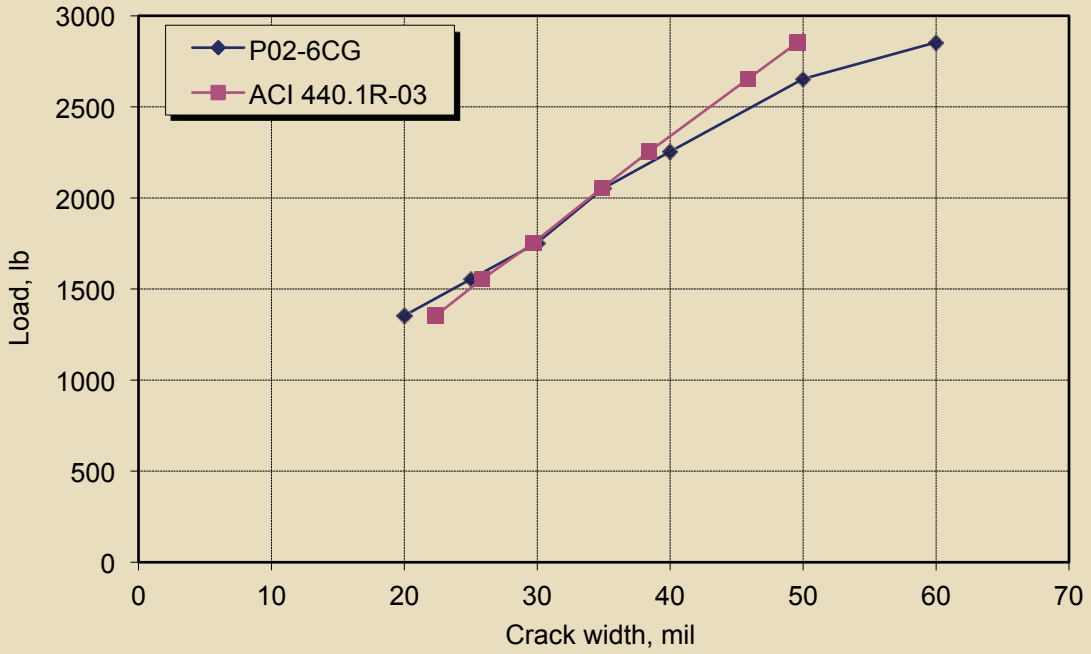

Figure 20. Load–crack width curve for poles reinforced with 6 carbon-fiber-reinforced polymer (CFRP) bars. Note: 1 mil = 0.0254 mm; 1 lb = 4.448 N.

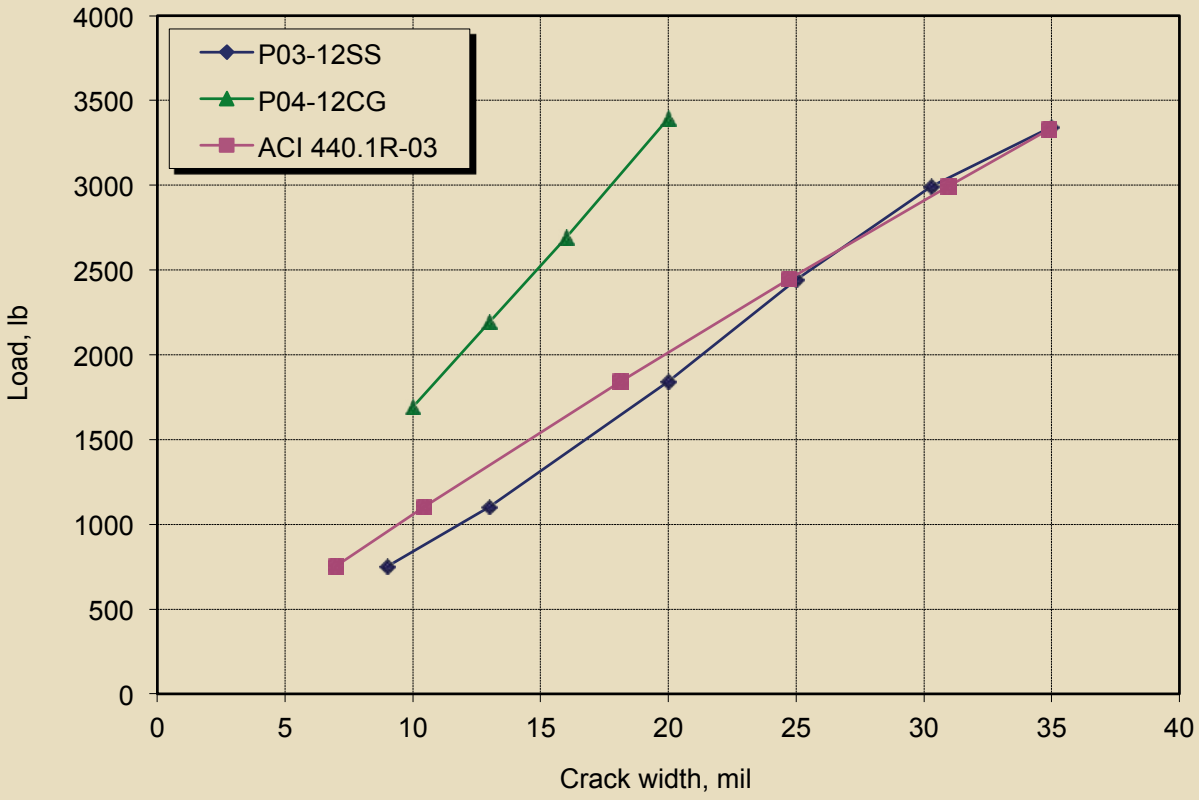

Figure 21. Load–crack width curve for poles reinforced with 12 carbon-fiber-reinforced polymer (CFRP) bars. Note: 1 mil = 0.0254 mm; 1 lb = 4.448 N.

fective moment of inertia were developed for spun concrete poles reinforced with CFRP bars.

- It is recommended that Eq. (2) be used for calculating the deflection of concrete poles reinforced with CFRP bars.
- The ACI 440.1R-03 crack width equation did not accurately predict experimental behavior in some cases. Although the experimental data were limited, it appears that a new ACI 440.1R-03 equation is needed for round cross sections.
- Additional tests with different reinforcement ratios will provide more information that will help in better understanding the flexural behavior of spun concrete poles reinforced with CFRP.

Acknowledgments

The research was performed in the structures laboratory of the Civil Engineering Department at the University of Alabama at Birmingham. The authors acknowledge Valmont-Newmark Co. for its technical and financial support in manufacturing the test specimens for the experimental study. Also, the authors acknowledge TechFab LLC for donating the CFRP grid used in this study.

References

1. Lyons, P. J. 2003. Feasibility Study of CFRP Prestressed Spun Cast Concrete Poles for Transmission Line Support. M.S. thesis, Department of Civil, Construction, and Environmental Engineering, University of Alabama.

2. Terrasi, G. P., and J. M. Lees. 2003. CFRP Prestressed Concrete Lighting Columns. In *Field Applications of FRP Reinforcement: Case Studies*, pp. 55–74. Farmington Hills, MI: American Concrete Institute (ACI).

3. Shalaby, A., H. F. Fouad, and R. Albanese. 2008. Flexural Behavior of Spun Concrete Poles Reinforced with CFRP Bars. In *Proceedings of the 54th PCI Annual Convention, Orlando, Florida*. CD-ROM.

4. Shalaby, A., and H. F. Fouad. 2009. Effective Moment of Inertia for Circular Concrete Members Reinforced with CFRP bars. In *Proceedings of the 55th PCI Annual Convention, San Antonio, Texas*. CD-ROM.

5. Oliphant, W. H., and C. J. Wong. 2002. Spun Concrete Poles for Electrical Transmission Structure Applications—Continuing to Push the Envelope of the Technology. In *Proceedings of the Electrical Transmission in a New Age*, pp. 241–248. American Society of Civil Engineers, Omaha, NE.

6. Fouad, Fouad H., Doug Sherman, and Rolf J. Werner. 1992. Spun Prestressed Concrete Poles—Past, Present, and Future. *Concrete International*, V. 14, No. 11 (November): pp. 25–29. Farmington Hills, MI: ACI.

7. Rodgers, Thomas E., Jr. 1984. Prestressed Concrete Poles: State-of-the-Art. *PCI Journal*, V. 29, No. 5 (September–October): pp. 52–103.

8. Fouad, H. F., L. N. Scott, E. Calvert, and M. Donovan. 1994. Performance of Spun Prestressed Concrete Poles During Hurricane Andrew. *PCI Journal*, V. 39, No. 2 (March–April): pp. 102–110.

9. ASTM Subcommittee A01.05. 2007. *Standard Specification for Steel Wire, Plain, for Concrete Reinforcement*. ASTM A82/A82M-07. West Conshohocken, PA: ASTM International.

10. ACI Committee 318. 2008. *Building Code Requirements for Structural Concrete (ACI 318-08) and Commentary (ACI 318R-08)*. Farmington Hills, MI: ACI.

11. ACI Committee 440. 2003. *Guide for the Design and Construction of Concrete Reinforced with FRP Bars.* ACI 440.1R-03. Farmington Hills, MI: ACI.

12. ACI Committee 440. 2006. *Guide for the Design and Construction of Concrete Reinforced with FRP Bars.* ACI 440.1R-06. Farmington Hills, MI: ACI.

13. PCI Committee on Prestressed Concrete Poles. 1997. Guide for the Design of Prestressed Concrete Poles. *PCI Journal*, V. 42, No. 6 (November–December): pp. 94–134.

14. Benmokrane, B., O. Chaallal, and R. Masmoudi. 1996. Flexural Response of Concrete Beams Reinforced with FRP Reinforcing Bars. *ACI Structural Journal*, V. 93, No. 1 (January): pp. 46–55.

15. Theriault, M., and B. Benmokrane. 1998. Effects of FRP Reinforcement Ratio and Concrete Strength on Flexural Behavior of Concrete Beams. *ASCE Journal of Composites for Construction*, V. 2, No. 1 (February): pp. 7–16.

16. Toutanji, H. A., and M. Saafi. 2000. Flexural Behavior of Concrete Beams Reinforced with Glass Fiber-Reinforced Polymer (GFRP) Bars. *ACI Structural Journal*, V. 97, No. 5 (September): pp. 712–719.

17. Branson, D. E. 1963. *Instantaneous and Time-Dependent Deflections of Simple and Continuous Reinforced Concrete Beams*. HPR report no. 7, part 1. Auburn, AL: Department of Civil Engineering and Auburn Research Foundation of Auburn University.

18. Yost, J. R., S. P. Gross, and D. W. Dinehart. 2003. Effective Moment of Inertia for Glass Fiber-Reinforced Polymer Reinforced Concrete Beams. *ACI Structural Journal*, V. 100, No. 6 (November): pp. 732–739.

19. Mota, C., S. Alminar, and D. Svecova. 2006. Critical Review of Deflection Formulas for FRP-RC Members. *ASCE Journal of Composites for Construction*, V. 10, No. 3 (May–June): pp. 183–194.

20. Bischoff, P. H., and A. Scanlon. 2007. Effective Moment of Inertia for Calculating Deflections of Concrete Members Containing Steel Reinforcement and Fiber-Reinforced Polymer Reinforcement. *ACI Structural Journal*, V. 104, No. 1 (January): pp. 68–75.

Notation

A = effective tension area of concrete with the same centroid as the tensile reinforcement farthest from neutral axis

A_a = area of the annulus

A_f = cross-sectional area of the FRP reinforcement

A_{fi} = area of the i^{th} reinforcement

A_{fu} = ultimate tensile strength of the FRP reinforcement

A_g = gross area of the cross section

c = location of the neutral axis measured from the extreme compression fiber of the pole

C_c = compression force

d_c = distance from the centroid of the effective tension area of concrete to the extreme tensile fiber of the cross section

d_i = distance of the i^{th} reinforcement from the extreme compression fiber

e_i = distance of the i^{th} reinforcement to the neutral axis

e_t = distance from the neutral axis to the extreme tensile reinforcement bar

E_c = modulus of elasticity of concrete

E_f = modulus of elasticity of FRP bars

E_s = modulus of elasticity of the steel bars

f'_c = cylinder compressive strength of concrete at 28 days

f_{fei} = stress of the i^{th} reinforcement

f_{en} = stress in extreme tensile reinforcement

f_{fu} = ultimate strength of the CFRP bars

f_r = modulus of rupture of concrete

I = moment of inertia of the cross section

I_{A_a} = moment of inertia of annulus calculated at the neutral axis

I_{cr} = cracking moment of inertia

I_e = effective moment of inertia of the cross section

I_g = gross moment of inertia of the section

k_b = bond coefficient for calculation of the crack width

Kc = position of the centroid of the stress block

L = length of the pole

M = applied moment

M_a = maximum moment applied to the pole

M_{cr} = cracking moment of concrete

M_u = ultimate moment capacity of the section

n_f = modular ratio between CFRP and concrete

T_f = tension force

w = crack width in mil

y_t = distance from the centroidal axis to the extreme tensile fiber of the section

x = distance from the support

α = reduction factor = 0.90

α_b = bond-dependent coefficient that was recommended to be equal to 0.5 until more data became available

β = ratio between the distance of the i^{th} reinforcement to the neutral axis and the distance of the extreme reinforcement bar to the neutral axis

β_1 = ratio of the depth of the equivalent rectangular stress block to the depth of the neutral axis

β_d = reduction coefficient for the effective moment of

inertia

Δ = deflection of the pole

η = moment of inertia coefficient

ρ = reinforcement ratio

ρ_b = balanced reinforcement ratio of the section

About the authors

Ashraf M. Shalaby, PhD, is a research assistant for the Department of Civil, Construction, and Environmental Engineering at the University of Alabama at Birmingham.

Fouad H. Fouad, PhD, P.E., is chair and professor of the Department of Civil, Construction, and Environmental Engineering at the University of Alabama at Birmingham. He is a fellow of ACI and ASCE and chairman of the PCI Committee on Prestressed Concrete Poles.

Ronald Albanese, P.E., MSCE, is a senior engineer for Valmont-Newmark in Birmingham, Ala. He is a member of the PCI Committee on Prestressed Concrete Poles.

Synopsis

Prestressed spun concrete poles are used primarily for supporting electric power transmission lines and distribution and for area lighting. In many applications they are placed directly in brackish water or saltwater, resulting in deterioration of the concrete pole due to steel corrosion.

A new type of reinforcement that can provide the desired structural characteristics and at the same time address the issue of corrosion is needed. Carbon fiber-reinforced polymer (CFRP) composites show potential as a replacement for steel reinforcement because of their corrosion resistance, high strength, and light weight that enables easier handling and reduces the self-weight of structures. The main objective of the research was to study the strength and deflection behavior of spun concrete poles with CFRP reinforcing bars. The study showed that the performance of the poles reinforced with CFRP bars was satisfactory under bending loads, which are the primary governing loads in most applications.

Keywords

Carbon-fiber-reinforced polymers, CFRP, cracking, deflection, flexure, FRP, moment capacity, poles.

Review policy

This paper was reviewed in accordance with the Precast/Prestressed Concrete Institute's peer-review process.

Reader comments

Please address any reader comments to journal@pci.org or Precast/Prestressed Concrete Institute, c/o *PCI Journal*, 200 W. Adams St., Suite 2100, Chicago, IL 60606.